ROYAL SOCIETY
OF CHEMISTRY

COMMUNICATION

Check for updates

Ferumoxytol of ultrahigh magnetization produced by hydrocooling and magnetically internal heating co-precipitation†

Bo Chen,[a] Jianfei Sun, ID *[a] Fengguo Fan,[a] Xiangzhi Zhang,[b] Zhiguo Qin,[a] Peng Wang,[c] Yang Li,[a] Xiquan Zhang,[d] Fei Liu,[d] Yanlong Liu,[d] Min Ji[a] and Ning Gu ID *[a]

Ferumoxytol, which is originally intended for MRI and anemia treatment, is currently the only inorganic nanodrug approved by FDA for clinical application *in vivo*. Common ferumoxytol seems incapable of meeting the requirements for diverse applications. Thus, the development of a novel strategy based on co-precipitation to produce ferumoxytol with high quality is an imminent task. Herein, we proposed a physically assisted strategy, namely hydrocooling and magnetically internal heating co-precipitation, to optimize the properties of ferumoxytol and thus significantly enhance its magnetic performance. Magnetization of the newly developed ferumoxytol can reach $104-105$ emu g^{-1} Fe, which is the highest value among the reported results. It has been found that the crystalline structures of the newly developed ferumoxytol have been greatly improved on the basis of pharmaceutical quality criteria.

Alternating magnetic field plays a critical role during the production process, which, on the one hand, results in thermogenesis of magnetic nanoparticles to self-ripen nanocrystal growth and, on the other hand, drives magnetic moments of seeds to unanimously align to enhance the crystallization and magnetism. By modification with hydrocooling, the importance of magnetically internal heating is highlighted. Our study reveals the significance of field assistance in the production of clinical inorganic nanodrugs, which will greatly enrich the clinical translation of magnetic inorganic nanodrugs.

[a] Jiangsu Key Laboratory for Biomaterials and Devices, Department of Biological Science and Medical Engineering, Southeast University, Nanjing 210009, P. R. China. E-mail: sunzaghi@seu.edu.cn, guning@seu.edu.cn
[b] Shanghai Synchrotron Radiation Facility, Shanghai Institute of Applied Physics, Chinese Academy of Sciences, Shanghai 201204, P. R. China
[c] Department of Sports Medicine and Adult Reconstructive Surgery, Drum Tower Hospital affiliated to Medical School of Nanjing University, Nanjing, 210008, P. R. China
[d] Research Institute of Chia Tai Tian Qing Pharmaceutical Group Limited by Share Ltd., Nanjing 210000, P. R. China
†Electronic supplementary information (ESI) available. See DOI: 10.1039/c8nr00736e

During the clinical translation of inorganic nanomaterials, one significant progress made in the past few decades is that certain iron oxide nanomaterials have been approved by FDA as nanodrugs to be used in human body.[1,2] The latest inorganic nanodrug approved by FDA is ferumoxytol, which is composed of an iron oxide core (7 nm in diameter) and a dextran (PSC) shell (20 nm in thickness), that acts as an MRI contrast agent and is used in the treatment of anemia.[3] However, as the translation of nanomedicine into the clinical trials is expanding,[4,5] ferumoxytol is facing increasing quality requirements for diverse applications; for instance, as an MRI contrast agent, ferumoxytol will cause a transition from the short-term enhancement of imaging signals in a specific organ to the long-term tracking of stem cellular fates *in vivo*.[6–9] Moreover, a novel magnetic particle imaging mode has been developed for iron oxide nanoparticle-specific tracking in deep tissues, which can realize the imaging for quantification with high sensitivity and high resolution and for quick-scan depending upon the high quality of magnetic nanoparticles.[10–14] These emerging applications require ferumoxytol to have good crystallinity, stable dispersivity, high magnetization, and preferably ordered spin orientation. However, ferumoxytol produced by a common production technique is incapable of meeting these demands. To boost the translation of this commercial nanodrug into diverse clinical applications, it is impending to develop an innovative strategy to effectively improve the properties of Ferumoxytol.

A common synthesis of ferumoxytol is based on the co-precipitation method because of the good controllability in term of biosafety. On account of the administrative regulation of clinical drugs, the alteration of the chemical recipe is impermissible. Generally, the co-precipitation preparation process can be divided into three parts: nucleation, growth, and ripening. Heating is the significant operation in the nanocrystal growth and ripening stages, which offers adequate energy to these two stages. If insufficient heat is supplied, particle growth will not proceed and the particles will have an inhomogeneous size distribution and poor crystallinity; this would result in an extremely low product quality. On the contrary,

heat is not necessary for the nucleation stage. After ammonia is added, the alkaline environment makes Fe^{3+}/Fe^{2+} react with OH- to form $Fe(OH)_3/Fe(OH)_2$ and then Fe_3O_4; Fe_3O_4 continues to generate in the solution until saturation, and Fe_3O_4 nanocrystals precipitate rapidly. This process is associated closely with pH and saturation degree regulation. Environmental temperature can influence various ferrite saturation degrees and further impact the nucleation. However, both low and high environmental temperature can lead to the completion of the nucleation stage. Thus, we resort to the physical method. Based on the growth mechanism of iron oxide nanoparticles synthesized by the co-precipitation method, the nanomaterials undergo a fast nucleation stage and an isotropic growth stage.[15,16] During the process, the presence of an external magnetic field has been proven to be propitious to the crystallization and magnetism of the products.[17] However, the direct imposition of a magnetostatic field on the reaction system often leads to the formation of chain-like or ring-like assemblies to minimize the systematic energy.[17–22] This case should obviously be avoided for the production of the nanodrug ferumoxytol.

Recently, alternating magnetic field (AMF) has been first employed to control the assembly of iron oxide nanoparticles by our group.[23] It has been discovered that the alternating magnetic field can even make the nanoparticles disperse more uniformly by controlling the frequency of the external field such that the magnetic moments of nanoparticles are kept parallel all the time within a period of AMF.[24,25] More importantly, magnetic nanoparticles can yield heat in the presence of AMF such that the generated seeds will heat up themselves. This thermogenesis can be employed for self-ripening during the growth stage of colloidal formation. To maximize the effect induced by the magnetically internal heating, low ambient temperature should be favorable. Actually, this operation has been applied for enhancing the crystallization of microscale crystals and nanocomposites.[26,27] Thus, if prolonged external hydrocooling can build an annealing environment, the AMF-assisted synthesis of ferumoxytol is speculated to be a positive feedback process, which will be favorable to obtain a ferumoxytol product with better crystallinity and magnetic property.

Herein, a novel strategy is reported to produce ferumoxytol with good crystallinity and higher magnetization, which involves magnetically internal heating during the co-precipitation process by imposing AMF, namely HMIHC (*i.e.*, hydrocooling and magnetically internal heating co-precipitation). We modified the common experimental setup of ferumoxytol production by reducing the ambient temperature with hydrocooling such that the nucleation and the growth stages of the formation of colloidal nanoparticles were separated. In the nucleation stage, a batch of seeds was formed and subsequently used in the growth stage. At this time, low ambient temperature inhibited the growth of the newly formed seeds. Moreover, the thermogenesis of nanoparticles activated the specific growth on the surfaces of these nanoparticles. This strategy somewhat resembles molecular beam epitaxy in mechanism.[28–30] The formation of colloidal nanoparticles now

is controlled by a kinetics process rather than a thermodynamics process in the common co-precipitation method; this will push the equilibrium of colloidal formation to shift towards the product direction. As a result, ferumoxytol with a better crystalline phase and higher magnetization can be obtained on the basis of pharmaceutical quality criteria. The results have confirmed our hypothesis and will open a new route to control the quality of magnetic nanocrystals with the co-precipitation method.

Experimental scheme is illustrated in Fig. 1. A reaction vial that was controllably cooled by an external hydrocooling bath was subjected to AMF of 790 kHz (Fig. 1). In our experiments, the ferumoxytol sample synthesized by the ordinary co-precipitation method and that synthesized by magnetically internal heat coprecipitation method without external hydrocooling (MIHC) were also prepared for comparison. In our experiments, Sample A denoted the ferumoxytol synthesized using the common co-precipitation method with 60 min for nucleation and ripeness. Sample B denotes ferumoxytol synthesized by the AMF-assisted co-precipitation method undergoing a fast temperature rising period of 60 min for nucleation and ripeness without external hydrocooling operation (MIHC). Sample C denotes ferumoxytol synthesized by the HMIHC method undergoing a slow temperature rising period of 180 min for nucleation and ripeness with an external hydrocooling operation.

The three synthesized samples were characterized to determine their composition. The results are shown in Fig. 2a, from which it can be seen that they are nearly identical in terms of iron-core size (about 7 nm) as basic pharmaceutical standards. ζ potential measurements showed that the three samples owned a similar surface electrical property in the suspension (Fig. S1†). The imposition of AMF was unable to cause the aggregation of magnetic nanoparticles. On the contrary, the size distribution of colloidal nanoparticles seemed to become increasingly uniform from Sample A to Sample C (Fig. S2†). Moreover, it was found the same amount of original reactants for the sample C yielded the maximal number of nanoparticles at the same Fe concentration (Fig. S3†). This result partly proved the abovementioned hypothesis that the magnetically internal heating combined with hydrocooling can boost the balance of colloidal formation to shift towards the products direction. Furthermore, the crystalline boundary and the arrangement of crystal lattice of Sample C seemed more distinct and regular than those of Sample A (Fig. 2a); this reflected that the crystallization of ferumoxytol was significantly improved. This result is in accordance with that hypothesized by the HMIHC method. Based on the explicit HRTEM image, the lattice parameter of ferumoxytol produced by HMIHC was 2.512 Å, matching well with the value of γ-Fe_2O_3 nanoparticles synthesized by the thermal decomposition method.[31–33] Moreover, the XRD, IR, and TGA results demonstrated that the three samples were extremely close to each other in term of their structural composition (Fig. 2b, c, and d). Concretely, X-ray diffraction patterns (Fig. 2c) demonstrated the same distinct characteristic diffraction 2θ angles of these
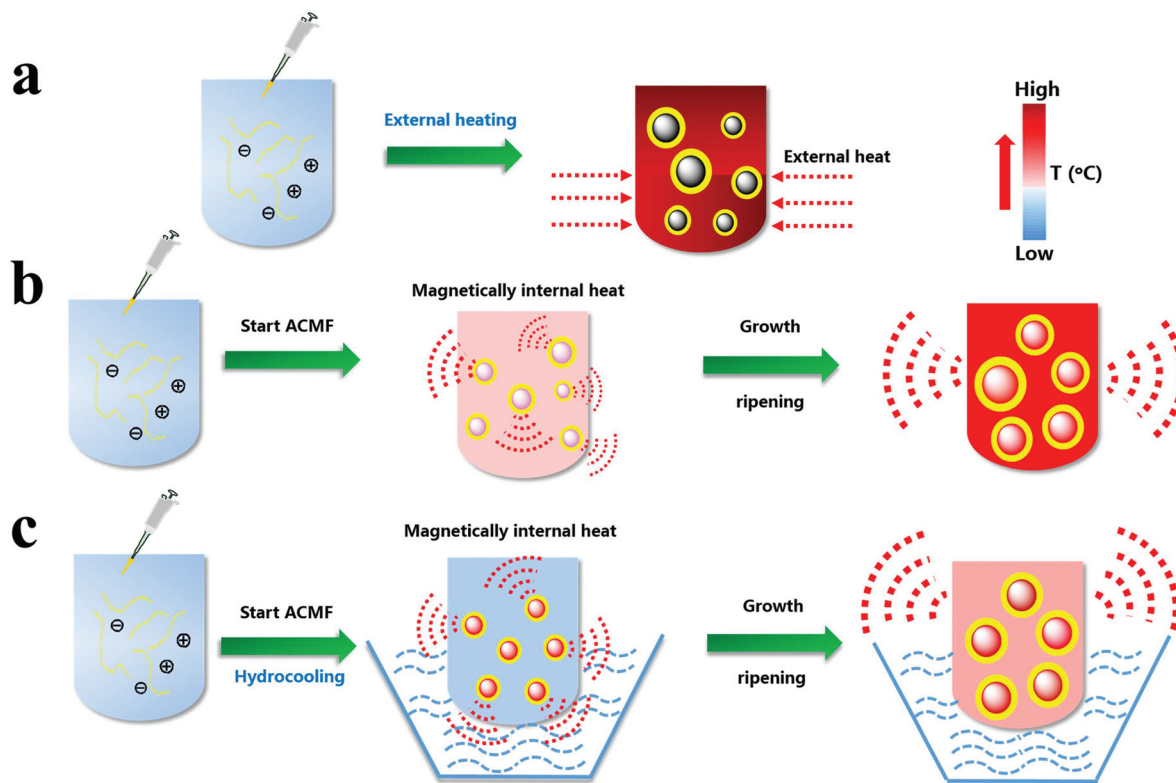
Fig. 1 Experimental schematic for the fabrication of (a) Sample A (by ordinary co-precipitation), (b) Sample B (by MIHC), and (c) Sample C (by HMIHC).
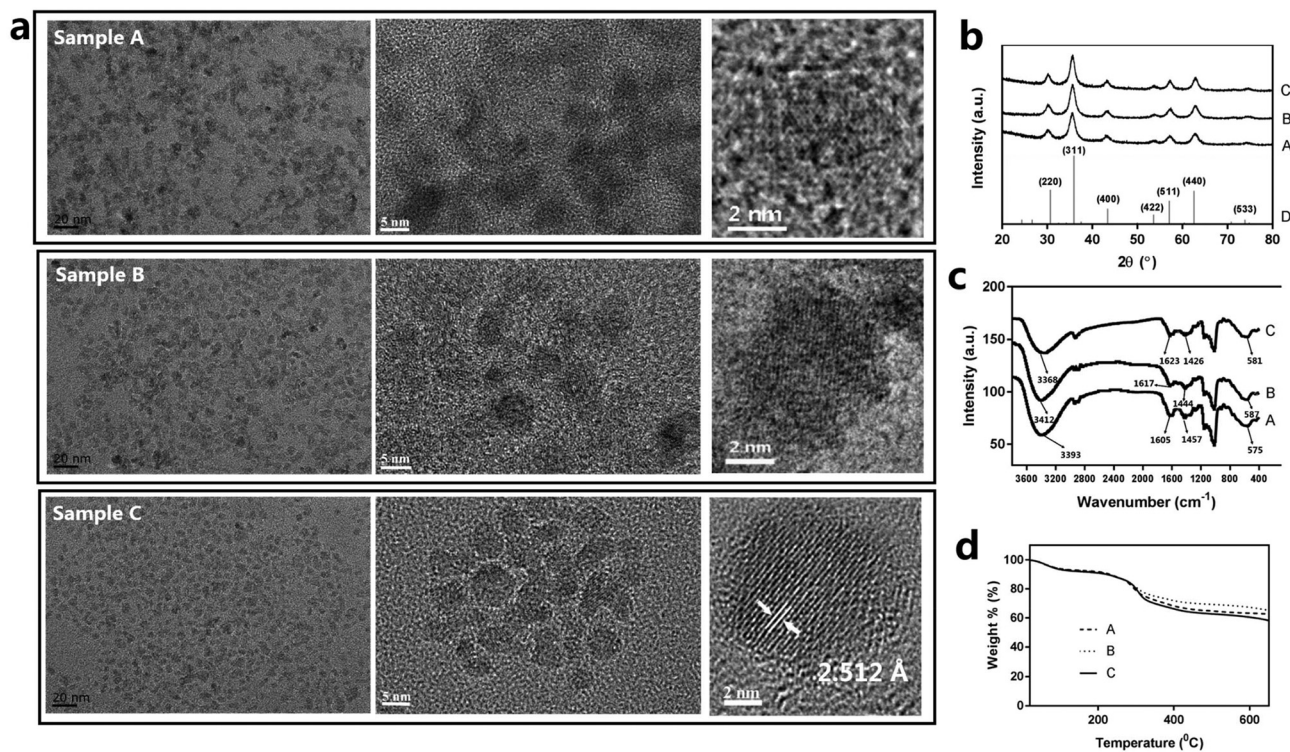

Fig. 2 Structural characterization of ferumoxytol: (a) TEM and HRTEM images of the ordinary coprecipitated Sample (A), MIHC Sample (B), and HMIHC Sample (C); (b) XRD profiles of Sample A–C and D (standard XRD pattern of γ-Fe$_2$O$_3$ crystal, JCPDS: 39-1346), (c) IR spectra of Sample A–C marked with the characteristic peaks, and (d) TGA analysis of Sample A–C.

particle crystals. Herein, 30.3°, 35.6°, 43.6°, 53.4°, 57.4°, and 63.0° are assigned to the (220), (311), (400), (422), (511), and (440) phases of the γ-Fe_2O_3 crystal (JCPDS: 39-1346), respectively.

Specifically, the band in the Fourier transform infrared spectrum (Fig. 2c) from 3200 cm^{-1} to 3400 cm^{-1} corresponds to the OH stretching vibration. The sharp COO^- specific stretching vibration peak is presented at 1610 cm^{-1}, and the multiple peaks around 1500 cm^{-1} shift to around 1440 cm^{-1}, manifesting that COO^- chelates with Fe ion. Furthermore, the absorption peak at 580 cm^{-1} is attributed to Fe_2O_3. According to the thermogravimetric curves (Fig. 2d), it was easy to speculate that crystallized water volatilized gradually below 300 °C; then, the coating material PSC began to decompose until around 550 °C, in the end, only iron oxide was left, and the particle weight remained unchanged. The results featured that the three sample owned an extremely similar structure with one third iron oxide in their weight. Some other necessary tests related to pharmaceutical quality have also verified that the newly developed ferumoxytol can meet the pharmaceutical standards (Table S1†) such that HMIHC will slightly affect the property of ferumoxytol as a nanodrug.

However, the alteration of magnetic property was significant. The measurements conducted *via* vibrating sample magnetometry demonstrated that the three samples were superparamagnetic (Fig. 3a). Surprisingly, the saturation magnetization of ferumoxytol produced by HMIHC can even reach 104–105 emu g^{-1} Fe (72–73 emu g^{-1} Fe_2O_3), much higher than that of ordinary ferumoxytol. The field cooling (FC) and zero field cooling (ZFC) curves of Sample A and Sample C are shown in Fig. 3b. The range of the testing temperature was from 10 K to 300 K, and the intensity of the applied magnetic field was 200 Oe. The FC and ZFC curves demonstrated a typical λ-shaped plot of superparamagnetic nanoparticles. As

seen from the FC curves, with a magnetic field of 200 Oe and temperature of 300 K, the magnetization of Sample C was almost quadruple than that of the Sample A; this confirmed the results obtained by VSM and the magnetic susceptibility detection in Fig. 3c. Since ferumoxytol produced by HMIHC owned a fairly good magnetostatic property, the alternating current magnetothermal performance was also expected to be good. Time-dependent thermogenic curves and two-dimensional thermal mapping for the three samples in the presence of a 380 kHz AMF are depicted in Fig. 3d, exhibiting that the magnetothermal performance is gradually enhanced from Sample A to C. Sample C can be heated up to 70 °C in 12 min, much higher than the case of the other two samples. Based on the thermogenic data, Sample C was calculated to also own highest specific absorption rate (SAR); this meant that ferumoxytol produced by HMIHC could greatly improve the capability of magnetothermal conversion.

We believe that the enhancement of magnetic property resulted from the improved crystallization and colloidal uniformity. Frequency-resolved electron spin resonance (ESR) was used to investigate the coupling of magnetic moments, and the results are shown in Fig. 4a. It can be seen that the ESR curve of Sample C is significantly broadened as compared to that of Sample A; this indicates the presence of a strong spin–spin coupling inside the nanoparticles.[34,35] Herein, it was thought that the spins should form a ring-like coupling rather than a head-to-tail coupling because the dipolar interaction between magnetic moments can narrow the ESR curve.[36] We utilized an OOMMF software to simulate the transition of magnetic moment arrangement in the presence of AMF from a random state to an ordered state (Fig. 4b). It was inferred that the ring-like electric field would lead to the vortex-like arrangement of the spins. Furthermore, X-ray magnetic circular dichroism (XMCD) technique was employed to detect the
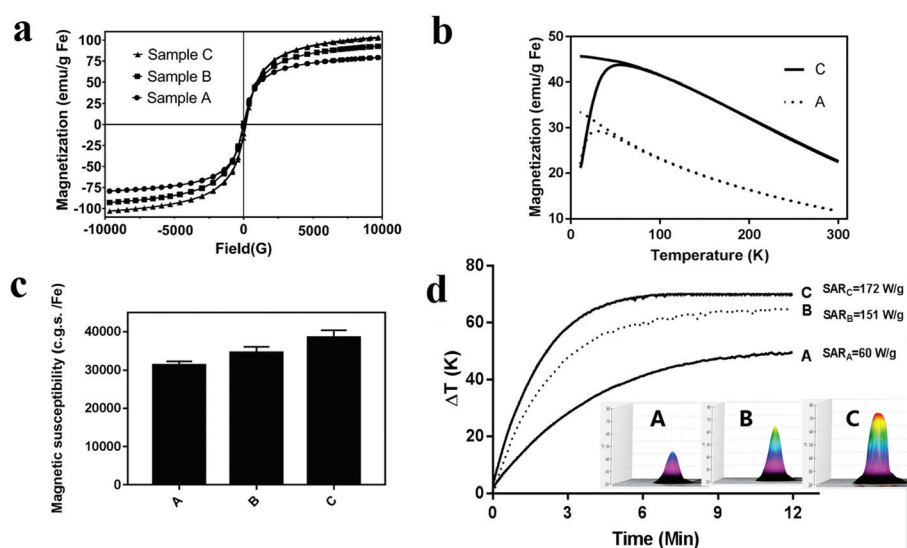

Fig. 3 Magnetization and magnetocaloric properties of Sample A–C: (a) field-dependent hysteresis loops (*M*–*H*) at room temperature, (b) ZFC and FC curves of Sample A and C (*H* = 200 Oe), (c) magnetic susceptibility values (*N* = 3), (d) time-dependent temperature curves and three-dimensional infrared images when the samples were located in AMF for 12 min at 380 kHz and 12 A at 10 mg mL^{-1} Fe.
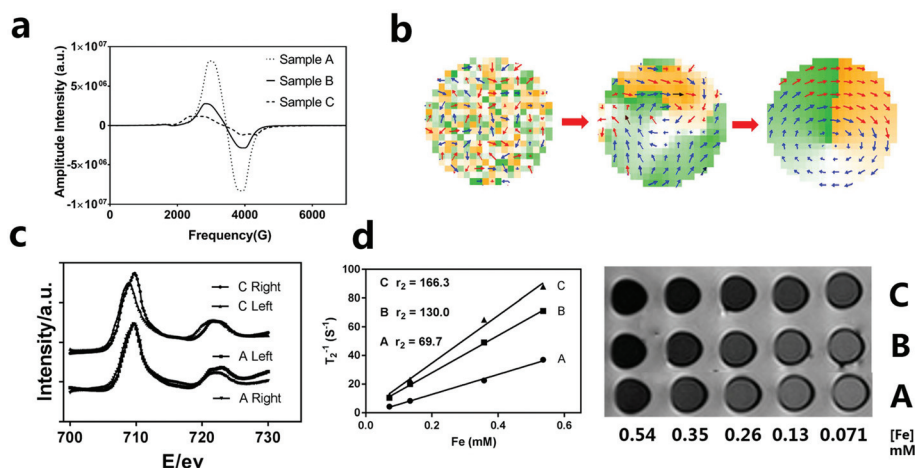
Fig. 4 Electromagnetic properties and magnetic imaging performance of Sample A–C: (a) frequency-dependent electron paramagnetic resonance intensity curves, (b) micromagnetic simulation for particle magnetic induction circular electric current formation in AMF at frequency of 790 kHz, (c) X-ray magnetic circular dichroism absorption intensity comparison of Sample A and Sample C ("Right" denotes the right-rotation light absorption and "Left" denotes the left-rotation light absorption), (d) Fe concentration-dependent reciprocal of transverse relaxation time plot, T_2 relaxivity calculation, and T_2-weighted magnetic resonance images in a 1.5 T MR scanner.

arrangement of magnetic moments.[37–39] It was found that Sample C showed an obvious difference when it was treated by left-handed rotation light and right-handed rotation light, whereas Sample A showed a little alteration (Fig. 4c). This result indicated that the magnetic moments of ferumoxytol produced by HMIHC were chiral-arranged, whereas the magnetic moments of common ferumoxytol were disordered. Due to the emergence of magnetic chirality, the coupling between the spins of Sample C should be vortex-like. The result was in accordance with the hypothesis that the spins formed the vortex-like pattern. The possibility for the formation of vortex-like spin coupling rooted in the ring-like induction electric field from the AMF. On the one hand, the electric field has been proven to be able to control the spin above the room temperature.[40–43] On the other hand, the induction electric field of AMF was shown to be capable of driving the nanoparticles into the formation of the vortex-like assemblies.[44] It was inferred that the small crystal seeds formed in the nucleation stage can aggregate into the vortex-like micro-structures under the treatment of the induction electric field. Then, in the growth stage, this micro-structure will play a role as a template to restrict the spins into the same arrangement and finally evolving into a nanoparticle.

Since ferumoxytol produced by HMIHC showed a better crystalline structure and magnetic property, the performance of the nanodrug in the magnetism-based applications was expected to be more promising. T_2-Weight MRI images with the three samples exhibited that Sample C could realize the same T_2 signal intensity/grey level and imaging contrast effect with the minimal amount of ferumoxytol (Fe concentration of 0.26 mM). By comparison, a double dose of the common ferumoxytol was needed to achieve the same result. The results are shown in Fig. 4d. Better crystallinity makes the structure more stable, and few iron ions leak from the particle. Therefore, the

nanoparticle may present favorable impacts as a whole entity without an influence from free iron ions. Based on these analyses, we infer that ferumoxytol obtained by the HMIHC method may be more facile for uptake and longer clearance *in vivo* due to its good crystallinity and stable structure. For the further contrast effect observation, an experiment with the microinjection of ferumoxytol into a rat brain has been carried out. Distinctly, Sample C demonstrated a stronger T_2 signal intensity in the local brain area than Sample A (Fig. S4†). The abovementioned results proved that a lower dosage of ferumoxytol produced by HMIHC can play the same role as the common ferumoxytol; this is obviously favorable for the safety of a nanodrug in clinical application and the long-term tracking of the imaging signals.

Moreover, the microwave absorption performance was tested, and the results are shown in Fig. S5.† Sample C showed strong microwave absorption in the low-frequency range from 6 to 12 GHz, and a broad band around the maximal absorption frequency. However, the effective absorption of Sample A occurred in the high-frequency range from 15 to 18 GHz. The variation also resembled the alteration trend of alternating current resistance (Fig. S5†). The impedance intensity from Sample A to Sample C decreased gradually. This result indicated that the electromagnetic property of ferumoxytol produced by HMIHC in the high-frequency range could also be tuned more flexibly than that of the common ferumoxytol, which will be favorable to the electromagnetic property-based applications.

The monitored temperature curve during the synthesis process is shown in Fig. 5a. It can be seen that the temperature quickly rose up to over 80 °C in the absence of hydrocooling. Herein, the reaction system quickly reached the thermodynamic equilibrium. Then, the growth stage was a thermodynamically controlled process. However, in the presence of hydrocooling, the whole reaction system was at about 0 °C for
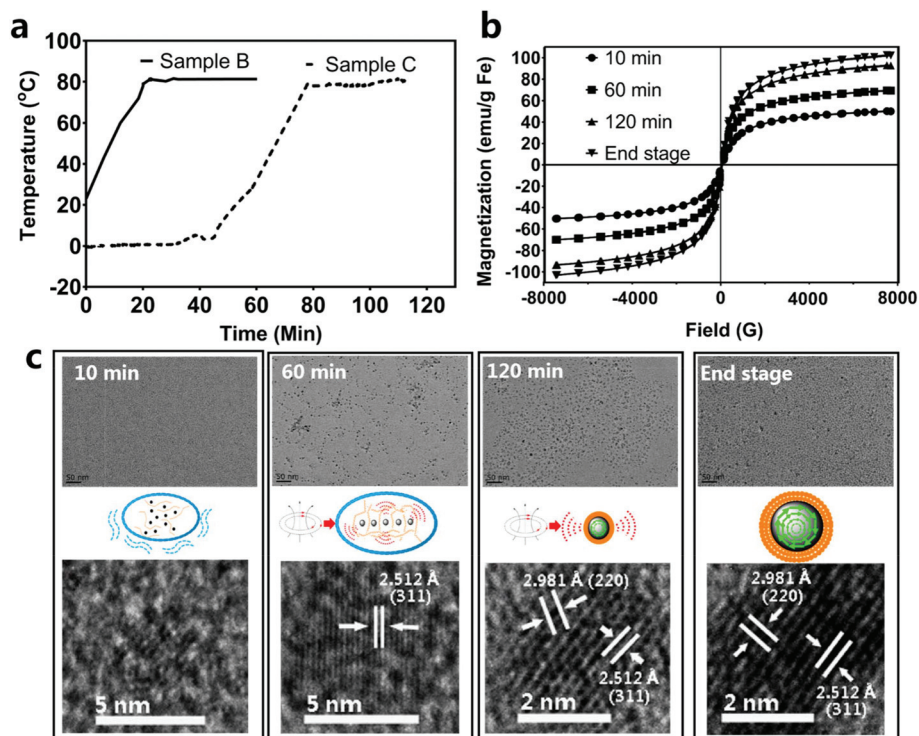
Fig. 5 (a) Temperature changing curve during the synthesis process of Sample B and Sample C. (b) Field-dependent hysteresis loops (*M*–*H*) at room temperature of the samples extracted at 10 min, 60 min, 120 min, and the end stage in the Sample C synthesis process. (c) TEM and HRTEM images of the samples extracted at 10 min, 60 min, 120 min, and the end stage in the Sample C synthesis process.

nearly 60 min and then rose up to 80 °C. During the beginning period, the major event was nucleation, which resulted in the formation of a number of small crystal nucleus. Herein, the magnetism of small crystal nucleus was relatively weak such that the major effect from the alternating magnetic field was the magnetic effect rather than the thermal effect. With the slow growth of small crystal nucleus, the magnetism was enhanced, and the thermogenesis in the presence of alternating magnetic field was increasingly augmented. Then, the crystal nucleus grew into colloidal nanoparticles in a gradually rapid manner. Therefore, this was a kinetically controlled process, which was more suitable to achieve crystalloids of higher quality. The analysis of intermediate products at each step of the synthesis process of Sample C confirmed this point. The TEM observation and HRTEM characterization of the products extracted at 10 min, 60 min, 120 min, and the end of the reaction process are shown in Fig. 5c. Moreover, selected area electron diffraction (SAED) patterns for these products are presented in Fig. S7.† The lattice spacings corresponding to the (220) and (311) crystal facets were measured as 2.981 and 2.512 Å, which were consistent with the XRD characteristic peaks at 30.3° and 35.6° (JCPDS: 39-1346), respectively. Based on the TEM observation, at the beginning stage, the size of iron oxide crystal seeds was merely 2 nm, and these seeds were highly uniform bathed *via* hydrocooling (10 min). At this time, the AMF prevented them from aggregation by inducing a repulsive interaction between parallel magnetic moments. As

the temperature slowly increased to 20 °C (60 min), the tiny crystal seeds grew into spherical nanoparticles with a diameter of 5 nm, which seemed still uniform. In this stage, the induction electric field began to induce the magnetic moments to arrange into a vortex-like pattern. Herein, with an increase in size, the thermogenesis of nanoparticles in the presence of AMF was also augmented; this would boost the ripening of nanoparticles (120 min). At the late growth stage, the size of nanoparticles reached 6–7 nm. When the aging process ended, the final size of the nanoparticles was about 8 nm, and the iron oxide nanoparticles were increasingly yielded. The growth of ferumoxytol produced by HMIHC was a positive feedback process, continuously impelling the balance to shift towards the direction of yielding the products because of the more and more thermogenesis with an increase in colloidal size. Herein, if hydrocooling is absent, too high ambient temperature will shield the reaction system from the influence of autologous heating of nanoparticles such that the growth process of ferumoxytol will be a thermodynamics process rather than a kinetic process. The VSM measurements also confirmed that the magnetism of nanoparticles became increasingly strong as the reaction proceeded (Fig. 5b). Additionally, we synthesized ferumoxytol *via* HMIHC in the presence of an AMF of 380 kHz. The sample also had advantages over the common ferumoxytol in terms of crystallinity and magnetism. However, the sample was inferior to Sample C; this indicated that the high frequency of AMF was favorable to the HMIHC method (Fig. S8†).

Conclusions

In summary, a novel strategy is proposed to produce an iron oxide inorganic nanodrug, ferumoxytol, by modifying the common co-precipitation method with a combination of the hydrocooling and the magnetically internal heating in the presence of an alternating magnetic field, namely HMIHC. With this strategy, ferumoxytol with highest magnetization as compared to the current reports was obtained. Ferumoxytol produced by HMIHC showed significantly improved colloidal crystallization and magnetic performance. The mechanism may lie in the role of AMF. On the one hand, the AMF was favorable to the crystallization and could prevent the nanoparticles from aggregation. Its induction electric field possibly induced the spins to form the vortex-like coupling rather than the head-to-tail coupling such that the stability and the magnetism were greatly enhanced. On the other hand, our strategy felicitously took advantage of the thermogenesis of iron oxide nanoparticles in the presence of an AMF. The autologous heating of nanoparticles rather than ambient heating may alter the colloidal growth stage from a thermodynamics process to a kinetic process such that the reaction can be more thorough and the produced ferumoxytol is of better crystallization and more yielding efficiency. Thus, the idea to exploit the autologous thermogenesis of nanoparticles to regulate the quality of materials is highly innovative (Fig. 6). We believe that this strategy is favorable to develop the novel nanodrug ferumoxytol with flexible magnetism and will boost the clinical translation of inorganic nanodrugs (Table 1).

Fig. 6 (a) Mechanism illustration of hydrocooling and magnetically internal heating co-precipitation synthesis for magneto-enhancing ferumoxytol. (b) Common ferumoxytol growth and ripening mechanism for the classical co-precipitation method. (c) Magneto-enhancing ferumoxytol growth and ripening mechanism for HMIHC.

Table 1 Magnetization comparisons of several marketed magnetic nanodrugs for clinical applications

Product name	Magnetization (emu g^{-1} Fe) at 0.1 Tesla	Magnetization (emu g^{-1} Fe) at 5 Tesla
Ferumoxytol obtained by HMIHC	**61.0 ± 0.7**	**105.0 ± 0.7**
Commercial ferumoxytol[45]	51	94
Ferumoxides[46]	37.0 ± 0.6	93.6 ± 1.6
Ferumoxtran-10[46]	53.6 ± 0.4	94.8 ± 0.7
Ferumoxsil[46]	49.4 ± 0.1	91.1 ± 0.2

Conflicts of interest

There are no conflicts to declare.

Acknowledgements

References

1 G. B. Toth, C. G. Varallyay, A. Horvath, M. R. Bashir, P. L. Choyke, H. E. Daldrup-Link, E. Dosa, J. P. Finn, S. Gahramanov, M. Harisinghani, I. Macdougall, A. Neuwelt, S. S. Vasanawala, P. Ambady, R. Barajas, J. S. Cetas, J. Ciporen, T. J. DeLoughery, N. D. Doolittle, R. W. Fu, J. Grinstead, A. R. Guimaraes, B. E. Hamilton, X. Li, H. L. McConnell, L. L. Muldoon, G. Nesbit, J. P. Netto, D. Petterson, W. D. Rooney, D. Schwartz, L. Szidonya and E. A. Neuwelt, *Kidney Int.*, 2017, **92**, 47–66.

2 A. M. El-Toni, M. A. Habila, J. P. Labis, Z. A. Alothman, M. Alhoshan, A. A. Elzatahry and F. Zhang, *Nanoscale*, 2016, **8**, 2510–2531.

3 Y. Liu, F. Yang, C. X. Yuan, M. X. Li, T. T. Wang, B. Chen, J. Jin, P. Zhao, J. Y. Tong, S. H. Luo and N. Gu, *ACS Nano*, 2017, **11**, 1509–1519.

4 Q. Wang, B. Chen, M. Cao, J. Sun, H. Wu, P. Zhao, J. Xing, Y. Yang, X. Zhang, M. Ji and N. Gu, *Biomaterials*, 2016, **86**, 11–20.

5 Q. Wang, B. Chen, F. Ma, S. Lin, M. Cao, Y. Li and N. Gu, *Nano Res.*, 2017, **10**, 626–642.
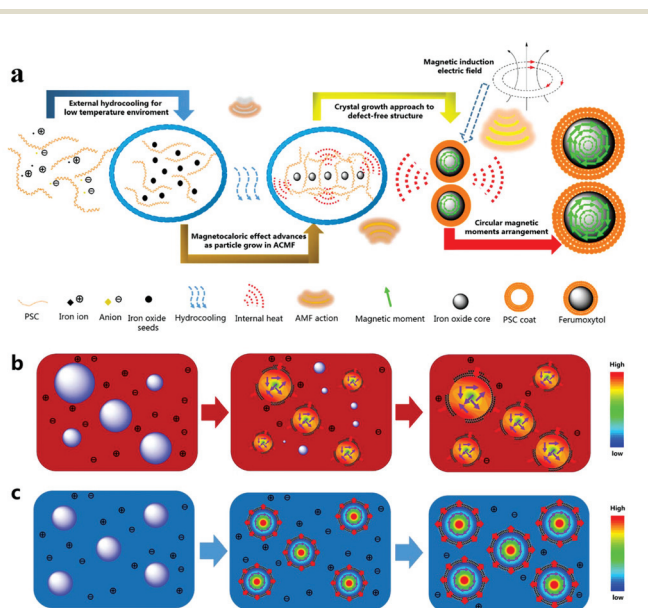
6 J. J. Lamanna, J. Gutierrez, L. N. Urquia, C. V. Hurtig, E. Amador, N. Grin, C. N. Svendsen, T. Federici, J. N. Oshinski and N. M. Boulis, *Stem Cells Transl. Med.*, 2017, **6**, 139–150.

7 C. Stirrat, S. R. Alam, T. J. MacGillivray, C. D. Gray, M. R. Dweck, S. Mirsadraee, S. Semple, P. A. Henriksen and D. E. Newby, *Eur. Heart J.*, 2015, **36**, 353–354.

8 S. C. Carreira, J. P. K. Armstrong, A. M. Seddon, A. W. Perriman, R. Hartley-Davies and W. Schwarzacher, *Nanoscale*, 2016, **8**, 7474–7483.

9 A. P. Khandhar, P. Keselman, S. J. Kemp, R. M. Ferguson, P. W. Goodwill, S. M. Conolly and K. M. Krishnan, *Nanoscale*, 2017, **9**, 1299–1306.

10 R. R. Jin, B. B. Lin, D. Y. Li and H. Ai, *Curr. Opin. Pharmacol.*, 2014, **18**, 18–27.

11 M. L. Wegscheid, R. A. Morshed, Y. Cheng and M. S. Lesniak, *Expert Opin. Drug Delivery*, 2014, **11**, 957–975.

12 C. Kaittanis, T. M. Shaffer, A. Ogirala, S. Santra, J. M. Perez, G. Chiosis, Y. M. Li, L. Josephson and J. Grimm, *Nat. Commun.*, 2014, **5**, 9.

13 W. Wu, C. Z. Jiang and V. A. L. Roy, *Nanoscale*, 2016, **8**, 19421–19474.

14 J. Sherwood, K. Lovas, M. Rich, Q. Yin, K. Lackey, M. S. Bolding and Y. Bao, *Nanoscale*, 2016, **8**, 17506–17515.

15 V. K. Lamer and R. H. Dinegar, *J. Am. Chem. Soc.*, 1950, **72**, 4847–4854.

16 Y. Wu, D. S. Wang and Y. D. Li, *Sci. China Mater.*, 2016, **59**, 938–996.

17 L. Hu, R. R. Zhang and Q. W. Chen, *Nanoscale*, 2014, **6**, 14064–14105.

18 L. Li, Y. Yang, J. Ding and J. M. Xue, *Chem. Mater.*, 2010, **22**, 3183–3191.

19 J. Sun, Y. Zhang, Z. Chen, H. Zhou and N. Gu, *Angew. Chem., Int. Ed.*, 2007, **46**, 4767–4770.

20 J. E. Martin and A. Snezhko, *Rep. Prog. Phys.*, 2013, **76**, 6601.

21 M. Krajewski, *Nanoscale*, 2017, **9**, 16511–16545.

22 V. Malik, A. Pal, O. Pravaz, J. J. Crassous, S. Granville, B. Grobety, A. M. Hirt, H. Dietsch and P. Schurtenberger, *Nanoscale*, 2017, **9**, 14405–14413.

23 P. Wang, J. Sun, Z. Lou, F. Fan, K. Hu, Y. Sun and N. Gu, *Adv. Mater.*, 2016, **28**, 10801.

24 B. Chen, Y. Li, X. Zhang, F. Liu, Y. Liu, M. Ji, F. Xiong and N. Gu, *Mater. Lett.*, 2016, **170**, 93–96.

25 Y. Li, K. Hu, B. Chen, Y. J. Liang, F. G. Fan, J. F. Sun, Y. Zhang and N. Gu, *Colloids Surf., A*, 2017, **520**, 348–354.

26 D. Ito, S. Yokoyama, T. Zaikova, K. Masuko and J. E. Hutchison, *ACS Nano*, 2014, **8**, 64–75.

27 Y. Cao, W. Geng, R. Shi, L. Shang, G. I. N. Waterhouse, L. Liu, L.-Z. Wu, C.-H. Tung, Y. Yin and T. Zhang, *Angew. Chem., Int. Ed.*, 2016, **55**, 14952–14957.

28 J. Demuth, E. Fahrenkrug, L. Ma, T. Shodiya, J. I. Deitz, T. J. Grassman and S. Maldonado, *J. Am. Chem. Soc.*, 2017, **139**, 6960–6968.

29 R. B. Yang, N. Zakharov, O. Moutanabbir, K. Scheerschmidt, L.-M. Wu, U. Goesele, J. Bachmann and K. Nielsch, *J. Am. Chem. Soc.*, 2010, **132**, 7592.

30 S. M. Poh, S. J. R. Tan, X. Zhao, Z. Chen, I. Abdelwahab, D. Fu, H. Xu, Y. Bao, W. Zhou and K. P. Loh, *Adv. Mater.*, 2017, **29**, 1605641.

31 E. Taboada, E. Rodriguez, A. Roig, J. Oro, A. Roch and R. N. Muller, *Langmuir*, 2007, **23**, 4583–4588.

32 A. Demortiere, P. Panissod, B. P. Pichon, G. Pourroy, D. Guillon, B. Donnio and S. Begin-Colin, *Nanoscale*, 2011, **3**, 225–232.

33 F. T. Parker, M. W. Foster, D. T. Margulies and A. E. Berkowitz, *Phys. Rev. B: Condens. Matter Mater. Phys.*, 1993, **47**, 7885–7891.

34 D. M. Jnaneshwara, D. N. Avadhani, B. D. Prasad, B. M. Nagabhushana, H. Nagabhushana, S. C. Sharma, C. Shivakumara, J. L. Rao, N. O. Gopal, S. C. Ke and R. P. S. Chakradhar, *J. Magn. Magn. Mater.*, 2013, **339**, 40–45.

35 J. Wilcoxen, S. Arragain, A. A. Scandurra, E. Jimenez-Vicente, C. Echavarri-Erasun, S. Pollmann, R. D. Britt and L. M. Rubio, *J. Am. Chem. Soc.*, 2016, **138**, 7468–7471.

36 B. Dobosz, R. Krzyminiewski, G. Schroeder and J. Kurczewska, *J. Phys. Chem. Solids*, 2014, **75**, 594–598.

37 P. Gambardella, A. Dallmeyer, K. Maiti, M. C. Malagoli, W. Eberhardt, K. Kern and C. Carbone, *Nature*, 2002, **416**, 301–304.

38 P. Gambardella, S. Rusponi, M. Veronese, S. S. Dhesi, C. Grazioli, A. Dallmeyer, I. Cabria, R. Zeller, P. H. Dederichs, K. Kern, C. Carbone and H. Brune, *Science*, 2003, **300**, 1130–1133.

39 Z. H. Sun, Q. H. Liu, T. Yao, W. S. Yan and S. Q. Wei, *Sci. China Mater.*, 2015, **58**, 313–341.

40 T. Zhao, A. Scholl, F. Zavaliche, K. Lee, M. Barry, A. Doran, M. P. Cruz, Y. H. Chu, C. Ederer, N. A. Spaldin, R. R. Das, D. M. Kim, S. H. Baek, C. B. Eom and R. Ramesh, *Nat. Mater.*, 2006, **5**, 823–829.

41 K. Shibuya and A. Sawa, *Adv. Electron. Mater.*, 2016, **2**, 1500131.

42 N. P. Lu, P. F. Zhang, Q. H. Zhang, R. M. Qiao, Q. He, H. B. Li, Y. J. Wang, J. W. Guo, D. Zhang, Z. Duan, Z. L. Li, M. Wang, S. Z. Yang, M. Z. Yan, E. Arenholz, S. Y. Zhou, W. L. Yang, L. Gu, C. W. Nan, J. Wu, Y. Tokura and P. Yu, *Nature*, 2017, **546**, 124.

43 L. M. Wang, O. Petracic, E. Kentzinger, U. Rucker, M. Schmitz, X. K. Wei, M. Heggen and T. Bruckel, *Nanoscale*, 2017, **9**, 12957–12962.

44 J. Sun, J. Dong, D. Sun, Z. Guo and N. Gu, *Langmuir*, 2012, **28**, 6520–6526.

45 H. Wei, O. T. Bruns, M. G. Kaul, E. C. Hansen, M. Barch, A. Wisniowska, O. Chen, Y. Chen, N. Li, S. Okada, J. M. Cordero, M. Heine, C. T. Farrar, D. M. Montana, G. Adam, H. Ittrich, A. Jasanoff, P. Nielsen and M. G. Bawendi, *Proc. Natl. Acad. Sci. U. S. A.*, 2017, **114**, 2325–2330.

46 C. W. Jung and P. Jacobs, *Magn. Reson. Imaging*, 1995, **13**, 661–674.